 © 2009 The Chemical Society of Japan

BCSJ Award Article

Macroscopic Phase Separation in a Tetraethoxysilane–Water Binary Sol–Gel System

Koichi Kajihara,* Shungo Kuwatani, Ryohei Maehana, and Kiyoshi Kanamura

Department of Applied Chemistry, Graduate School of Urban Enviromental Sciences, Tokyo Metropolitan University, 1-1 Minami-Osawa, Hachioji, Tokyo 192-0397

Received July 28, 2009; E-mail: kkaji@tmu.ac.jp

A procedure to prepare macroporous silica gels from an acid-catalyzed tetraethoxysilane (TEOS)–water binary system was developed, and the macroscopic morphology formation was examined at a range of conditions under controlled reaction temperature. This procedure involves two-step mixing of TEOS and water containing pH control agents. The gel morphology is significantly influenced by the solution composition in each mixing step, even if the overall solution composition is unchanged. The macroscopic morphology is formed by phase separation between hydrophobic silica oligomers modified by unhydrolyzed ethoxy groups and hydrophilic solvent mixture consisting of water and ethanol generated from TEOS. The morphology can be described as an aggregation of macroscopic particles, which are most likely formed by the spinodal decomposition and subsequent fragmentation of the silica-rich phase occurring at the solvent-rich side of a miscibility gap. The resultant macroporous gels are dried in a relatively short time to obtain crack-free monolithic silica xerogels, which are useful as silica glass precursors.

Sol–gel synthesis of silicates has been extensively studied, mainly because the precursors (silicon alkoxides) are easy to handle due to their moderate reactivity and their various derivatives including those modified with organic functional groups are commonly available. Sol–gel method is widely used to form various functional silicates, such as monolithic gels and glasses, films, and powders.[1]

In the sol–gel method silica glasses are obtained by sintering monolithic silica xerogels. The low processing temperature as compared with vapor-phase and conventional fusion methods is beneficial in suppressing devitrification and weight loss during manufacturing of silica glasses. However, the utility of the sol–gel method is limited by fracture associated with shrinkage during drying, which originates from evaporation induced capillary force and its inhomogeneous propagation in gel monoliths.[1] The capillary force is decreased by decreasing the surface tension of pore liquid and the inhomogeneous shrinkage is suppressed by slowing down the drying. Thus, various techniques, including careful control of drying conditions,[2–5] incorporation of solvents of low surface tension (often termed "drying control chemical additives," DCCAs),[6–8] and supercritical drying,[9] have been developed to obtain monolithic silica xerogels. The capillary force is also decreased by increasing the pore size. A notable approach is dispersing particulate silica fillers in the precursor solution.[10–15] In this method the pores can be easily enlarged by increasing the size of the fillers. Furthermore, the fillers mechanically strengthen the gel framework, making it possible to greatly alleviate the fracture problem. Another method is to utilize macropores formed by phase separation between silica gel and solvent phases. In alkoxide-based gelling systems macroscopic phase separation is induced by incorporating additives such as organic polymers,[16,17] polar organic solvents (e.g., formamide and methanol),[18,19] and a large amount of strong acids.[20]

Unhydrolyzed alkoxides are hydrophobic and incompatible with water-rich hydrophilic solvent mixtures.[21] Thus, by finely tuning the degree of hydrolysis, macroscopic phase separation may be induced without additives. Indeed, macroscopic phase separation is observed in trimethoxymethylsilane (methyltrimethoxysilane, MTMS)–water binary systems[19] because the methyl group in MTMS is unhydrolyzable and maintains the silica oligomer hydrophobicity even in water-rich conditions. A similar mechanism accounts for the phase separation of a mixture of tetramethoxysilane (TMOS) and polar organic solvents occurring at a low ($\lesssim$2) water to TMOS molar ratio.[18–20,22] However, in additive-free tetraalkoxysilane-based systems macroscopic phase separation under water-rich conditions is unexplored.

A major challenge in inducing macroscopic phase separation in water-rich tetraalkoxysilane-based gelling systems is to maintain alkoxy groups partially unhydrolyzed. In our recent paper[23] it is realized using tetraethoxysilane (TEOS) introducing two key techniques: (i) two-step mixing that separates the partial hydrolysis and polycondensation stages, and (ii) formation of an acetate buffer system to stabilize pH of gelling solutions at weakly acidic pH, at which the hydrolysis is

Published on the web December 10, 2009; doi:10.1246/bcsj.82.1470

significantly slowed down whereas the polycondensation is fast.[1,24] This method is different from the preceding two-step acid–base hydrolysis method,[1,25] where the solution is basic and hydrolysis after the second mixing is not suppressed intentionally. Furthermore, this method does not need alcohols as external solvents, similar to its first demonstration in a non phase-separating TMOS–water system.[26] However, the details of the development of the macroporous morphology, which is necessary to optimize the preparation conditions of the xerogel monoliths, have not been studied.

The purpose of the present paper is to investigate the morphology formation in the TEOS–water binary system at various compositions under controlled reaction temperature.

Experimental

A plastic container containing 5.2 g of TEOS was placed in a water bath with a thermostat and kept at 10, 20, or 30 °C. A dilute aqueous solution of nitric acid was added and the mixture (solution 1) was stirred vigorously. Solution 1 became homogeneous and transparent in ca. 30–60 min.[27] The molar ratio of the components in solution 1 was $TEOS:H_2O:HNO_3 = 1:x_1:0.002$. In this study x_1 was smaller than 4, typically $x_1 \simeq 2$, to leave TEOS partially unhydrolyzed. The amount of nitric acid, which catalyzes the partial hydrolysis, was close to the necessity minimum to obtain such a clear solution within 60 min at 20 °C. After 60 min (20 or 30 °C) or 90 min (10 °C) stirring solution 1 was further mixed with an aqueous solution of ammonium acetate ($AcONH_4$) (solution 2) to form a clear solution with overall molar ratio of $TEOS:H_2O:HNO_3:AcONH_4 = 1:x_1 + x_2:0.002:y$. After 1 min stirring the stir bar was removed and the container was held in the water bath. The gelation and phase separation times (t_g and t_{ps}, respectively) were recorded as the time delay from the second mixing. t_g was defined as the moment at which the solution lost macroscopic fluidity. t_{ps} was similarly defined as the moment at which the solution lost transparency completely. The resultant gel was aged for 1 day at 60 °C. Then the solvent was disposed and the gel was gently dried for 2 days at 60 °C. The dried gels were subjected to scanning electron microscope (SEM) observations. Several dried gels were calcined in air for 1 h at 300 °C and the mesoporous structure was characterized by nitrogen adsorption–desorption isotherms (BEL Japan Inc., BELSORP-mini). The size distribution of the mesopores was calculated from the adsorption branch of the isotherm using the Barrett–Joyner–Halenda method.[28] Raman spectra of solution 1 before the second mixing were measured using a Fourier-transform infrared Raman spectrometer (Nicolet, Model 960).

Results

Figure 1 shows the appearance of dried gels of $x_1 + x_2 = 10$ and $y = 0.01$ prepared at 20 °C. Crack-free white xerogels were obtained at $x_1 = 1.8$ and 1.9, whereas the dried gels were translucent and broken into small pieces at $x_1 \geqq 2.0$. SEM images of the same gels are shown in Figure 2. The morphology of the gels can be depicted as particle aggregates. The particle size was ca. 50–100 nm at $x_1 \gtrsim 2.0$ and increased sharply with a decrease in x_1 at $x_1 < 2$.

First, the amount of ammonium acetate (y) and preparation temperature were optimized. The variation of gel morphology with y was examined for gels of $x_1 = 1.9$ and $x_1 + x_2 = 10$ prepared at 20 °C. Their average particle size, t_g, and t_{ps} are summarized in Figure 3. t_g and t_{ps} were nearly equal. They

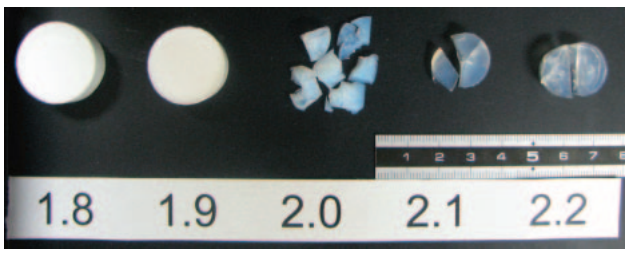

Figure 1. Photograph of dried gels of $x_1 + x_2 = 10$ and $y = 0.01$ prepared at 20 °C. The x_1 value of each gel is shown in the picture.

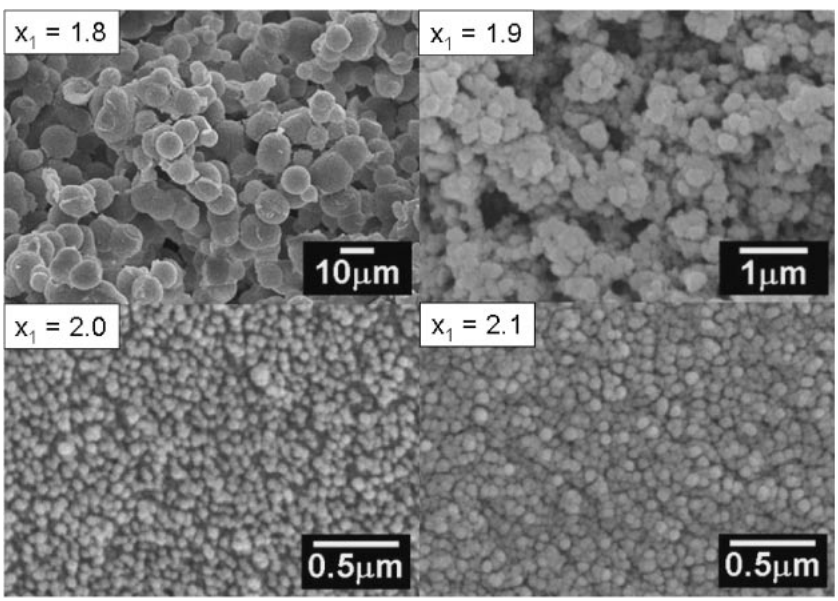

Figure 2. SEM images of dried gels of $x_1 + x_2 = 10$ and $y = 0.01$ prepared at 20 °C. The x_1 value of each gel is shown in the picture.

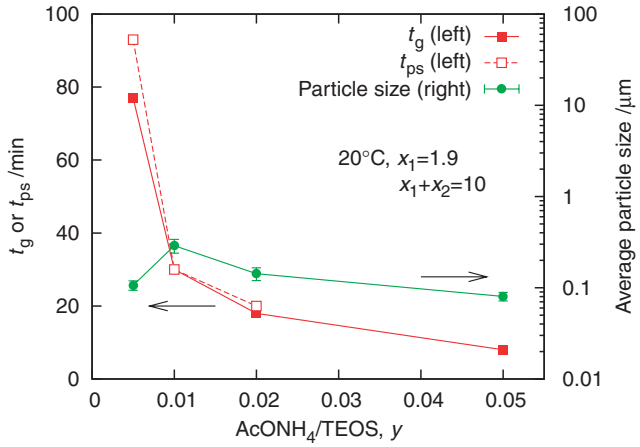

Figure 3. Variation of gelation and phase separation times with y for gels of $x_1 = 1.9$ and $x_1 + x_2 = 10$ prepared at 20 °C. Average particle size of the dried gels are also shown.

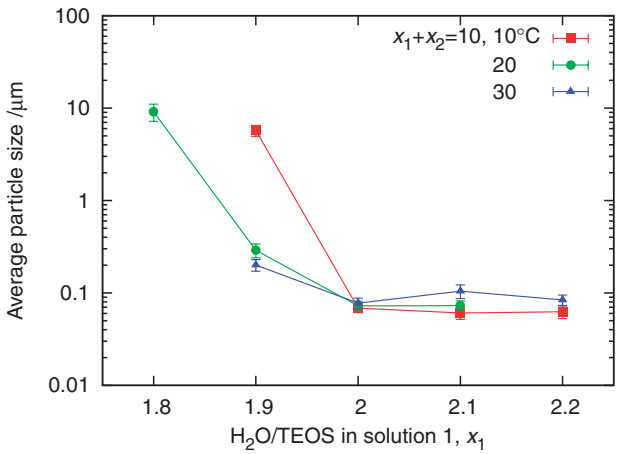

Figure 4. Temperature dependence of the average particle size of dried gels of $x_1 + x_2 = 10$ and $y = 0.01$. The error bar denotes the experimental uncertainty.

were relatively large at $y = 0.005$, whereas they decreased monotonically with an increase in y. At $y = 0.05$ the resultant gel was translucent and t_{ps} was not recorded. At $y = 0.01$, the average particle size was the largest. In addition, the use of ammonium acetate can be minimized without significantly slowing down the gelation.

Figure 4 summarizes the variation of the average particle size of dried gels with temperature for gels of $x_1 + x_2 = 10$ and $y = 0.01$. Although the particle size at $x_1 \lesssim 2.0$ decreased with an increase in temperature, the overall dependences of the particle size on x_1 were similar. Figure 5 shows the variation of t_g and t_{ps} with temperature. Both t_g and t_{ps} decreased with increasing temperature. At all temperatures t_g showed a maximum at $x_1 \simeq 2.0$–2.1. The phase separation was observed at $x_1 \leqq 1.9$. However, at $x_1 = 1.8$, the silica-rich phase was precipitated before the gelation at 10 °C, and solution 1 did not become homogeneous at 30 °C. Consequently, x_1 range to cause phase separation along with homogeneous gelation was the widest at 20 °C. Thus, the following experiments were performed at $y = 0.01$ and 20 °C.

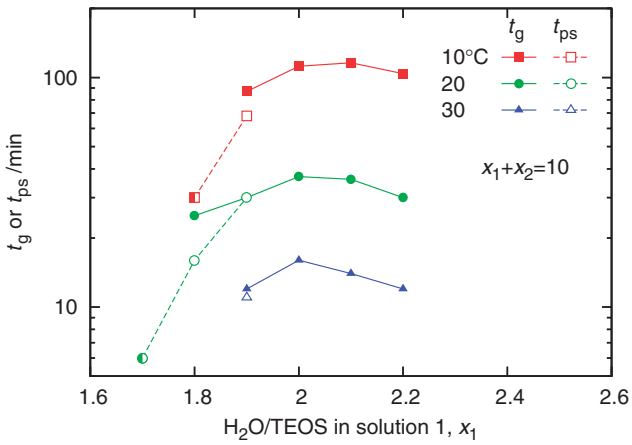

Figure 5. Temperature dependence of gelation and phase separation times of gels of $x_1 + x_2 = 10$ and $y = 0.01$. At compositions denoted by the half-filled symbols the silica-rich phase is precipitated at t_{ps} and the gelation time cannot be defined.

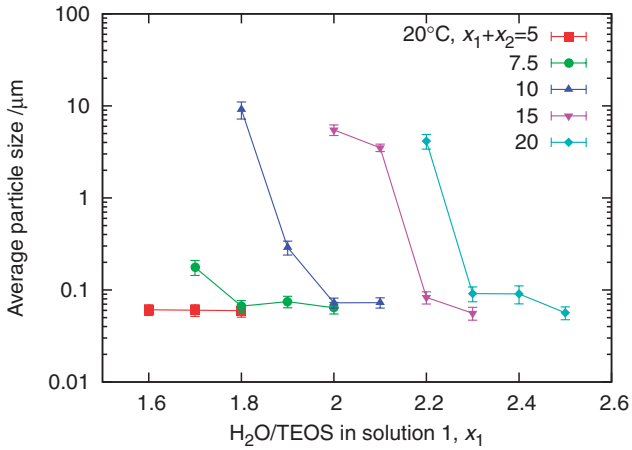

Figure 6. Compositional dependence of the average particle size of dried gels of $y = 0.01$ prepared at 20 °C. The error bar denotes the experimental uncertainty.

Figure 6 shows the dependence on solution composition of the average particle size evaluated from SEM images of gels prepared at $y = 0.01$ and 20 °C. The average particle size increased sharply at x_1 at which the appearance of the gel changed from translucent to opaque. As $x_1 + x_2$ decreased, this increase in the average particle size occurred at smaller x_1. This increase became less distinct at smaller $x_1 + x_2$, and was no longer observed at $x_1 + x_2 = 5$.

Figure 7 shows dependence of t_g and t_{ps} on solution composition. t_g showed a maximum against x_1 except at $x_1 + x_2 = 5$, where solution 1 did not become homogeneous at $x_1 \leqq 1.5$. As $x_1 + x_2$ increased t_g decreased and the maximum shifted to the larger x_1 side. The phase separation was observed at the left side of the x_1 maximum, and t_{ps} monotonically increased with an increase in x_1. At the left ends of the plots for gels of $x_1 + x_2 \geqq 7.5$, t_g was not defined because the phase separation was too fast and the silica-rich phase was precipitated before gelation.

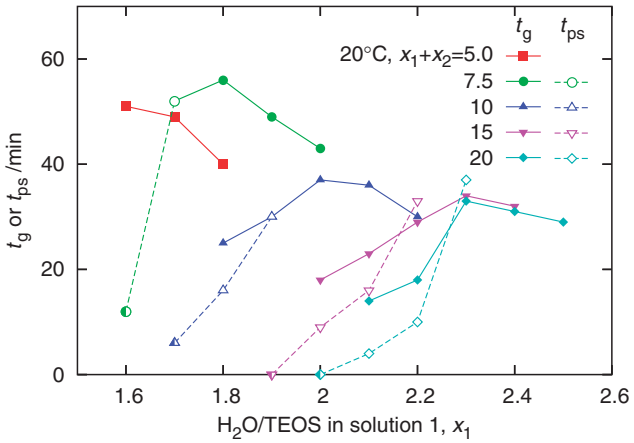

Figure 7. Compositional dependence of gelation and phase separation times of gels of $y = 0.01$ prepared at 20 °C. At compositions denoted by the half-filled symbols the silica-rich gel phase is precipitated at t_{ps} and the gelation time cannot be defined.

Figures 8a and 8b show the N_2 adsorption–desorption isotherms and pore size distribution curves of gels of $x_1 + x_2 = 10$ and $y = 0.01$ prepared at 20 °C and calcined in air at 300 °C. Both the pore size and volume increased with a decrease in x_1 from 2.2 to 1.9, most significantly between $x_1 = 2.0$ and 1.9. At $x_1 = 1.8$, the pore size and volume was the smallest but it was apparent because the gel was macroporous (Figure 2a) and the macropores are too large to be measured by N_2 adsorption. Figure 8c shows the pore size distribution curves of gels of $x_1 + x_2 = 5$ and $y = 0.01$. In this system the macroscopic phase separation was not observed (Figure 7). However, the pore size and volume slightly increased with a decrease in x_1 from 1.7 to 1.6, suggesting an onset of phase separation.

Figure 9 shows Raman spectra of solutions 1 stirred for 1 h at 20 °C since the first mixing. Raman spectra of TEOS and ethanol are also shown. Raman band A at ca. 680 cm^{-1} appeared only in solutions 1 and is attributed to Si–O–C stretching mode of monohydrolyzed TEOS, $(EtO)_3SiOH$.[1,23,29,30] This band gradually disappeared with an increase in x_1, representing a general tendency of the enhancement of hydrolysis. Bands B and C originate from ethoxy groups and were seen in all spectra. In ethanol, band B consists of two peaks at ca. 1050 and ca. 1100 cm^{-1}, attributed mainly to C–C–O asymmetric stretching and CH_3 rocking modes, respectively.[31–33] In contrast, TEOS shows a single peak at ca. 1090 cm^{-1},[34–36] probably because of the high energy shift of the C–C–O asymmetric stretching mode. Band C is mainly due to CH_2 twist mode,[31–33,35,36] and the peak position is slightly different between ethanol (ca. 1275 cm^{-1}) and TEOS (ca. 1295 cm^{-1}). Since in this system ethoxy groups are associated either with ethanol or with EtO–Si bonds, the peak decomposition of band B or C may yield the fraction of ethoxy groups attached to silicon, $f \equiv [\text{EtO–Si}]/([\text{EtO–Si}] + [\text{EtOH}])$. The Raman spectra of TEOS and ethanol can be used as standard spectra for the peak decomposition. Intensity ratio of the Raman signals of respective components, I_{TEOS}/I_{EtOH}, may be given by $I_{TEOS}/I_{EtOH} = af/(1 - f)$. The proportional

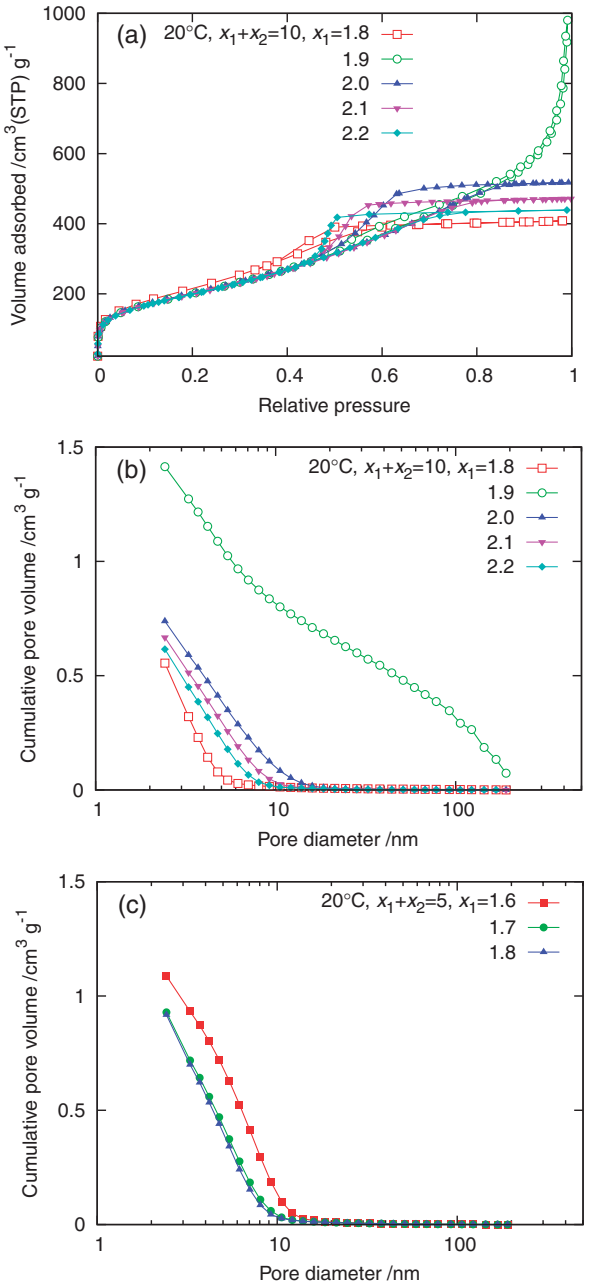

Figure 8. Nitrogen adsorption–desorption isotherms and pore size distributions of gels of $y = 0.01$ prepared at 20 °C and calcined at 300 °C. Isotherms (a) and pore size distributions (b) of gels of $x_1 + x_2 = 10$, and pore size distributions of gels of $x_1 + x_2 = 5$ (c) are shown.

factor a was determined using standard solutions with known ethanol to TEOS ratios. It was assumed that the Raman scattering cross sections of bands B and C for EtO–Si group are independent of the type of other functional groups attached to the same silicon atom. In this study band B was used because the baseline was relatively flat and the intensity was stronger than that of band C, making it possible to improve the accuracy of the peak decomposition.

Figure 10a shows the variation of f with x_1 and the inset shows an example of the peak decomposition. The standard spectra of TEOS and ethanol were synthesized using two and

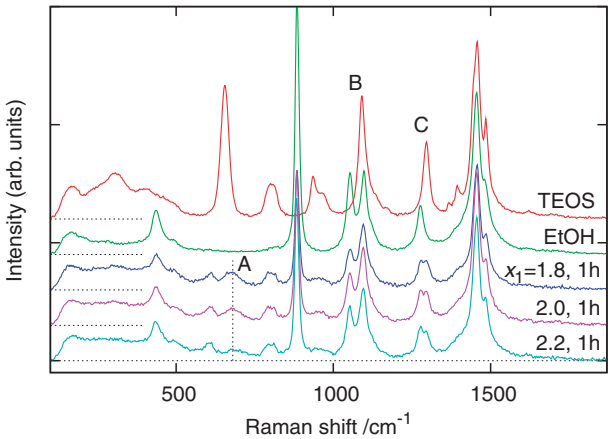

Figure 9. Raman spectra of solutions 1 at $x_1 = 1.8$, 2.0, and 2.2 measured after 1 h stirring at 20 °C. Raman spectra of TEOS and ethanol (denoted as EtOH) are also shown. The assignments of the bands A, B, and C are described in the text.

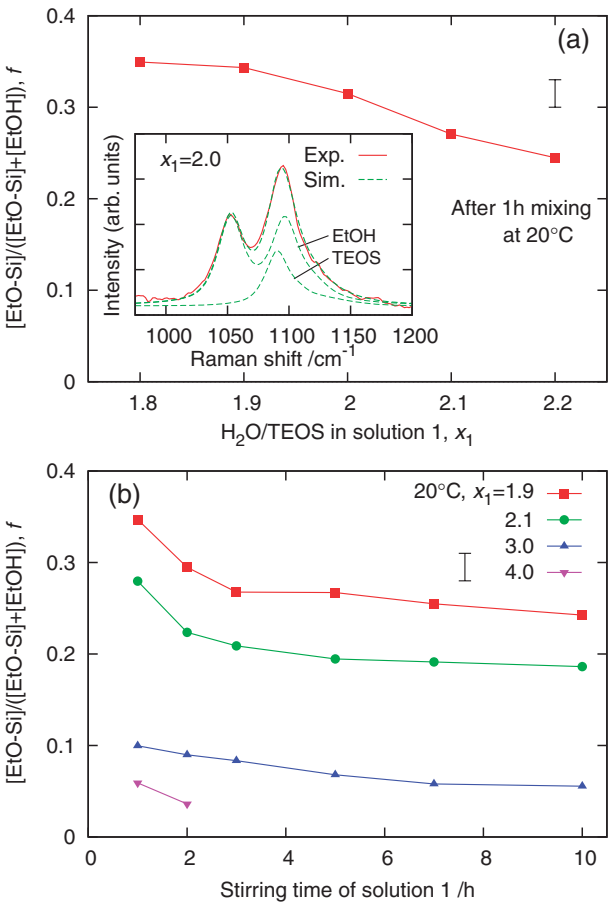

Figure 10. Dependence on x_1 (a) and stirring time (b) of the fraction of ethoxy groups attached to silicon, calculated by least-squares fitting of the Raman band at ca. 1100 cm^{-1} (band B in Figure 9) with a linear combination of the Raman bands of TEOS and ethanol. The inset of panel (a) shows an example of the peak decomposition, performed for the solution with $x_1 = 2.0$ after 1 h stirring. The error bars represent the experimental uncertainties.

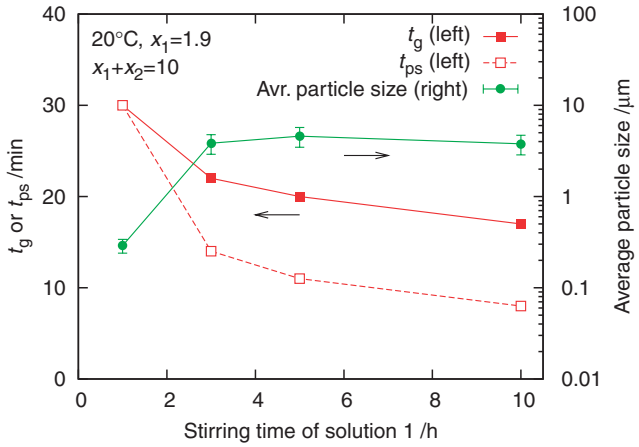

Figure 11. Variation of gelation and phase separation times with stirring time of solution 1 for gels of $x_1 = 1.9$, $x_1 + x_2 = 10$, and $y = 0.01$ prepared at 20 °C. Average particle size of the dried gels are also shown.

three pseudo Voigt functions, respectively, and their linear combination was least-squares fitted to the observed spectra to evaluate I_{TEOS}/I_{EtOH}. f decreased with an increase in x_1, and the decrease became significant at $x_1 \gtrsim 2$. Figure 10b shows the variation of f with stirring time of solution 1. At $x_1 = 1.9$ and 2.1, f decreased considerably with time up to ca. 3 h. However, subsequent decrease in f was slow and more than 20% of ethoxy groups remained unhydrolyzed even at 10 h. These two curves were almost parallel. The gap between them was relatively large as compared with that between $x_1 = 2.1$ and 3.0 or 4.0, suggesting that the variation of f with x_1 is the largest at $x_1 \simeq 2$. At $x_1 \gtrsim 3$, hydrolysis was almost completed after sufficiently long stirring.

Figure 11 shows variation of t_g and t_{ps} with stirring time of solution 1 for gels of $x_1 = 1.9$ and $x_1 + x_2 = 20$. Variation of the average particle size is also shown. The average particle size increased distinctly between 1 and 3 h, and was nearly unchanged after 3 h. In contrast, t_g decreased monotonically with stirring time even after 3 h. t_{ps} also decreased with time. t_{ps} was smaller than t_g after 3 h, consistent with the observation that the average particle size after 3 h was much larger than that at 1 h.

Discussion

Free energy of mixing ΔG of two types of polymers **1** and **2** is a function of their volume fraction ϕ_1 and ϕ_2, their degree of polymerization, P_1 and P_2, and their interaction parameters, χ_{12}. ΔG is estimated by the Flory–Huggins equation as[37]

$$\Delta G \propto RT\left(\frac{\phi_1}{P_1}\ln\phi_1 + \frac{\phi_2}{P_2}\ln\phi_2 + \chi_{12}\phi_1\phi_2\right) \quad (1)$$

where R is the gas constant and T is the absolute temperature. A positive χ_{12} indicates a repulsive interaction between polymers **1** and **2**. When ΔG is positive the mixture is decomposed into two phases. Equation 1 shows that ΔG can be positive when P_1 and P_2 are large and χ_{12} is positive and large.

The phase separation in conventional alkoxide-based gelling systems at a given composition (ϕ_1 and ϕ_2 are fixed) may be

described by substituting $P_2 = 1$ into eq 1 considering that the solvent molecules do not polymerize.[17,38] Thus, the phase separation is controlled by the time evolution of P_1 and χ_{12}. In a TEOS–water mixture P_1 corresponds to the degree of the polymerization of silica oligomer. χ_{12} is related to the hydrophobicity of silica oligomer and the hydrophilicity of solvent mixture consisting of water and ethanol originating from TEOS. In this study water to TEOS ratios in the first and second mixing steps (x_1 and x_2, respectively) independently modify P_1 and χ_{12}. Thus, the gel morphology is significantly different, even if the overall solution compositions are the same, as typically shown in Figure 1 and Figure 2.

x_1 is closely related to χ_{12}, because it determines the fraction of unhydrolyzed ethoxy groups f in solution 1 (Figure 10a). As x_1 decreases, f increases and the macroscopic phase separation becomes significant (Figure 1, Figure 2, and Figure 6). The upper limit of x_1 at which the phase separation is observed (x_{1c}, ca. 2 at $x_1 + x_2 = 10$) agrees well with the drop in f (Figure 10a). These observations confirm that repulsive interaction between hydrophobic silica oligomers and hydrophilic solvent mixture of water and ethanol is the main driving force for the phase separation. It is surprising that only ca. 10% decrease in f significantly changes the gel morphology. At $x_1 \gtrsim x_{1c}$ t_g decreases with an increase in x_1 (Figure 7) because of an increase in P_1 as a result of the enhancement of hydrolysis. However, this dependence of P_1 on x_1 does not explain the observed variation of morphology with x_1, indicating that the influence of P_1 on morphology formation is minor here. The decrease in t_g at $x_1 \lesssim x_{1c}$ is due to an enhancement of the polycondensation by phase separation, which concentrates silica oligomers in the silica-rich phase and increases their reaction probability.[16,39,40]

The domain size of macroscopic structure formed by spinodal decomposition is often sensitively influenced by small changes in initial conditions. The observed domain size changes drastically within a small x_1 range (Figure 6), suggesting that the phase separation mechanism is spinodal decomposition rather than nucleation-growth. The high sensitivity of the domain size on x_1 is similar to the results for water–formamide–TMOS systems,[17,18] where the spinodal decomposition occurs between polar hydrophilic solvent mixture and hydrophobic silica oligomer derived from TMOS.

$x_1 + x_2$ controls the hydrophilicity of solvent mixture. As $x_1 + x_2$ increases the fraction of ethanol, which is amphiphilic and increases the compatibility between TEOS and water, decreases. It would not significantly change the hydrophobicity of silica oligomer because the hydrolysis after the second mixing is slow. Thus, with increasing $x_1 + x_2$ it is expected that χ_{12} increases and the phase separation is enhanced. Indeed, x_{1c} increases with an increase in $x_1 + x_2$ (Figure 6), indicating that at larger $x_1 + x_2$ values less hydrophobic (larger x_1) silica oligomers undergo the phase separation.

$x_1 + x_2$ also determines ϕ_1 and ϕ_2. In this study the observed gel morphology is depicted by an aggregation of macroscopic particles (Figure 2), indicating that the silica-rich phase is the minor phase ($\phi_1 < \phi_2$) and undergoes fragmentation in the late stage of the phase separation.[17] Thus, by increasing ϕ_1, such fragmentation may be suppressed and gels with open framework structure may be obtained. ϕ_1 increases with decreasing $x_1 + x_2$. However, even at the lowest $x_1 + x_2$ limit ($x_1 + x_2 = 5$) gels with open framework structure could not be obtained.

At a fixed solution composition ($x_1 = 1.9$, $x_1 + x_2 = 10$) the phase separation is enhanced by extending the stirring time of solution 1 (Figure 11). It decreases f, with making the silica oligomer less hydrophobic and the solvent mixture ethanol rich. Since these changes decrease χ_{12}, the results cannot be explained in terms of χ_{12} change. In contrast, t_g monotonically decreases with time, suggesting an increase in P_1. Thus, the enhancement of the phase separation with stirring time is most likely due to an increase in P_1 (eq 1). The slight decrease in the domain size at 10 h may be due to a viscosity increase, which slows down the growth of the domains.

In this study ammonium acetate is used to increase pH after the second mixing. Ammonium acetate is a salt of a weak acid (acetic acid, $pK_a = 4.8$) and an acetate ion traps a proton originating from nitric acid as

$$AcO^- + H^+ \rightarrow AcOH \quad (2)$$

Since the amount of ammonium acetate is larger than that of nitric acid, the resultant solution contains both acetic acid and acetate ion, forming an acetate buffer system and stabilizing pH around weakly acidic pH range. The pH of the solution may be roughly given by

$$pH = pK_a + \log\left(\frac{[AcO^-]}{[AcOH]}\right) = 4.8 + \log\left(\frac{y - 0.002}{0.002}\right) \quad (3)$$

indicating that pH increases with an increase in y. Equation 3 predicts pH 5.0 at $y = 0.005$ and pH 6.2 at $y = 0.05$.

Figure 3 shows that t_g decreases with an increase in y. It is consistent with the observation that polycondensation is accelerated with an increase in pH up to ca. 7.[24] Thus, the decrease in the particle size at $y \gtrsim 0.01$ is explained by enhancement of the polycondensation and increase in the solution viscosity, which suppresses the phase separation. However, despite the t_g decrease the average particle size increases between $y = 0.005$ and 0.01. This observation suggests that at $y = 0.005$ pH after the second mixing is not high enough to sufficiently slow down the hydrolysis, resulting in a decrease in χ_{12}.

As temperature rises, the reaction probability increases and the polycondensation is accelerated. Indeed, t_g decreases significantly with an increase in temperature as shown in Figure 5. On the other hand, as temperature rises the compatibility of the mixture increases because of an increase in the mixing entropy. It probably corresponds to a decrease in the average particle size and a small shift of x_{1c} to lower x_1 (Figure 4), both of which indicate suppression of the phase separation. However, the effect of temperature on the morphology formation is minor compared to the variation of the morphology with the solution composition.

Conclusion

Macroporous silica gels are found to be prepared from an alcohol-free acid-catalyzed tetraethoxysilane (TEOS)–water binary system. This process consists of two-step mixing of TEOS with water. First, TEOS is partially hydrolyzed with acidic water. Then, by adding aqueous solution of a salt of a

weak acid (ammonium acetate) pH of the solution is stabilized in a weakly acidic pH range, utilizing the buffering effect of acetate compounds. This procedure slows down the subsequent hydrolysis of partially hydrolyzed TEOS, while increasing the water fraction of the solvent mixture. Thus, hydrophobic silica oligomers are formed in a water-rich hydrophilic solvent mixture, making it possible to induce macroscopic phase separation in parallel with gelation. The morphology formation was examined at various compositions under controlled temperature. The morphology of gels can be described as aggregation of macroscopic particles. The average particle size is influenced by the solution composition in each mixing step and cannot be defined only by the overall composition. The particle size varies two orders of magnitude with a slight change of the water to TEOS ratio in the first mixing step, suggesting that the phase separation mechanism is the spinodal decomposition. It is noteworthy that solution is homogeneously gelled in several tens of minutes at room temperature. The fast gelation, which is much faster than that of conventional acid-catalyzed TEOS-based gels, is beneficial in shortening the processing time. Furthermore, the starting composition is simple and alcohols that are commonly used in sol–gel reactions are unnecessary, making it possible to minimize the use of chemical reagents. The resultant macroporous gels can be easily dried without fracture, typically within a few days, facilitating the sol–gel synthesis of monolithic silica gels.

This work was partially supported by the Asahi Glass Foundation.

References

1 C. J. Brinker, G. W. Scherer, *Sol–Gel Science: The Physics and Chemistry of Sol–Gel Processing*, Academic Press, New York, **1990**.
2 M. Yamane, S. Aso, S. Okano, T. Sakaino, *J. Mater. Sci.* **1979**, *14*, 607.
3 M. Nogami, Y. Moriya, *J. Non-Cryst. Solids* **1980**, *37*, 191.
4 F. Kirkbir, H. Murata, D. Meyers, S. R. Chaudhuri, A. Sarkar, *J. Sol-Gel Sci. Technol.* **1996**, *6*, 203.
5 H. Murata, D. E. Meyers, F. Kirkbir, S. R. Chaudhuri, A. Sarkar, *J. Sol-Gel Sci. Technol.* **1997**, *8*, 397.
6 S. Wallace, L. L. Hench, *Mater. Res. Soc. Symp. Proc.* **1984**, *32*, 47.
7 T. Adachi, S. Sakka, *J. Mater. Sci.* **1987**, *22*, 4407.
8 T. Adachi, S. Sakka, *J. Non-Cryst. Solids* **1988**, *99*, 118.
9 S. S. Kistler, *J. Phys. Chem.* **1932**, *36*, 52.
10 R. D. Shoup, in *Ultrastructure Processing of Advanced Ceramics*, ed. by J. D. Mackenzie, D. R. Ulrich, Wiley, New York, **1988**, p. 347.
11 E. M. Rabinovich, D. W. Johnson, Jr., J. B. MacChesney, E. M. Vogel, *J. Am. Ceram. Soc.* **1983**, *66*, 683.
12 E. M. Rabinovich, J. B. Macchesney, D. W. Johnson, Jr., J. R. Simpson, B. W. Meagher, F. V. Dimarcello, D. L. Wood, E. A. Sigety, *J. Non-Cryst. Solids* **1984**, *63*, 155.
13 G. W. Scherer, J. C. Luong, *J. Non-Cryst. Solids* **1984**, *63*, 163.
14 R. Clasen, *J. Non-Cryst. Solids* **1987**, *89*, 334.
15 M. Toki, S. Miyashita, T. Takeuchi, S. Kanbe, A. Kochi, *J. Non-Cryst. Solids* **1988**, *100*, 479.
16 K. Nakanishi, N. Soga, *J. Am. Ceram. Soc.* **1991**, *74*, 2518.
17 K. Nakanishi, *J. Porous Mater.* **1997**, *4*, 67.
18 H. Kaji, K. Nakanishi, N. Soga, *J. Non-Cryst. Solids* **1995**, *181*, 16.
19 K. Nakanishi, K. Kanamori, *J. Mater. Chem.* **2005**, *15*, 3776.
20 H. Kozuka, S. Sakka, *Chem. Mater.* **1989**, *1*, 398.
21 H. D. Cogan, C. A. Setterstrom, *Chem. Eng. News* **1946**, *24*, 2499.
22 K. Nakanishi, N. Tanaka, *Acc. Chem. Res.* **2007**, *40*, 863.
23 K. Kajihara, M. Hirano, H. Hosono, *Chem. Commun.* **2009**, 2580.
24 C. J. Brinker, *J. Non-Cryst. Solids* **1988**, *100*, 31.
25 C. J. Brinker, K. D. Keefer, D. W. Schaefer, C. S. Ashley, *J. Non-Cryst. Solids* **1982**, *48*, 47.
26 D. Avnir, V. R. Kaufman, *J. Non-Cryst. Solids* **1987**, *92*, 180.
27 I.-G. Marino, P. P. Lottici, D. Bersani, R. Raschellà, A. Lorenzi, A. Montenero, *J. Non-Cryst. Solids* **2005**, *351*, 495.
28 E. P. Barrett, L. G. Joyner, P. P. Halenda, *J. Am. Chem. Soc.* **1951**, *73*, 373.
29 I. Artaki, M. Bradley, T. W. Zerda, J. Jonas, *J. Phys. Chem.* **1985**, *89*, 4399.
30 J. L. Lippert, S. B. Melpolder, L. M. Kelts, *J. Non-Cryst. Solids* **1988**, *104*, 139.
31 C. Tanaka, *Nippon Kagaku Kaishi* **1962**, *83*, 792.
32 J.-P. Perchard, M.-L. Josien, *J. Chim. Phys.* **1968**, *65*, 1856.
33 Y. Mikawa, J. W. Brasch, R. J. Jakobsen, *Spectrochim. Acta, Part A* **1971**, *27*, 529.
34 J. W. Ypenburg, H. Gerding, *Recl. Trav. Chim. Pays-Bas* **1972**, *91*, 1245.
35 M. C. Matos, L. M. Ilharco, R. M. Almeida, *J. Non-Cryst. Solids* **1992**, *147–148*, 232.
36 J. Gnado, P. Dhamelincourt, C. Pélégris, M. Traisnel, A. L. M. Mayot, *J. Non-Cryst. Solids* **1996**, *208*, 247.
37 P. J. Flory, *Principles of Polymer Chemistry*, Cornell University Press, Ithaca, New York, **1971**.
38 H. Kaji, K. Nakanishi, N. Soga, T. Inoue, N. Nemoto, *J. Sol-Gel Sci. Technol.* **1994**, *3*, 169.
39 K. Nakanishi, N. Soga, *J. Non-Cryst. Solids* **1992**, *139*, 1.
40 K. Nakanishi, H. Komura, R. Takahashi, N. Soga, *Bull. Chem. Soc. Jpn.* **1994**, *67*, 1327.